A hierarchical DCNN-based approach for classifying imbalanced water inflow in rock tunnel face

Jiayao Chen[a,b], Hongwei Huang[a], Anthony G. Cohn[b,c,d,e,f], Mingliang Zhou[a,1], Dongming Zhang[a], Jianhong Man[a]

[a] *Key Laboratory of Geotechnical and Underground Engineering of Ministry of Education and Department of Geotechnical Engineering, Tongji University, Shanghai 200092, China*
[b] *School of Computing, University of Leeds, LS2 9JT Leeds, United Kingdom*
[c] *Department of Computer Science and Technology, Tongji University, Shanghai 211985, China*
[d] *School of Civil Engineering, Shandong University, Jinan 250061, China*
[e] *Luzhong Institute of Safety, Environmental Protection Engineering and Materials, Qingdao University of Science and Technology, Zibo 255000, China*
[f] *School of Mechanical and Electrical Engineering, Qingdao University of Science and Technology, Qingdao 260061, China*

Abstract: Accurate water inflow assessment in the under-construction rock tunnel sites is critical for the next optimized construction and rehabilitation strategy. In this paper, a deep convolutional neural networks (DCNN)-based method, named H-ResNet-34, is implemented to classify water inflow category from rock tunnel faces in under-construction highway tunnels in Yunnan, China. An image database is compiled, which contains 8,000 images in five different water inflow categories of rock tunnel faces, namely complete dry (CD), wet state (WS), dripping state (DS), flowing state (FS) and gushing state (GS). Herein, a crucial issue is the imbalanced images between damage and non-damage owing to the vast sample of datasets and between various damages due to varying damage occurrence rates, which bring enormous challenges for conventional DCNN models. Thus, a hierarchical classification structure is applied to overcome the issue of imbalanced images at two different levels: coarse-level and fine-level. The coarse-level distinguishes the dataset with non-damage (i.e. complete dry) images. The fine-level computes the occurrence probability of the image dataset with water inflow damage. The constructed framework is then trained, validated, and tested using tunnel face images with various water inflow categories. The testing results suggest that the proposed hierarchical classifier is well competent for water inflow classification for rock tunnel face images and can effectively alleviate the imbalanced data issue.

Keywords: Water inflow, Rock tunnel, Image classification, Imbalanced images, Deep convolutional neural network

1. Introduction

The assessment of water inflow is critical for the final classification of surrounding rock in rock tunnels under construction, owing to its significant impact on constructors and managers in case of tunnel collapse and water gushing accidents. It also provides a significant basis for continuing project strategies under limited construction schedules and engineering budgets. In general, the manual water inflow inspection approaches (e.g., tipping buckets, discharge vessels, weirs, etc) (Rálek and Hokr, 2013), which are widely employed under current practice (Hwang and Lu, 2007). Although correct flow rate values can be obtained by these contact manners, they are labour- and time-consuming, and even threatening the safety of engineers (Fernandez and Moon, 2010). Thus, there is an urgent to explore a vision-based inspection method that can identify the water inflow categories accurately in rock tunnel faces (Chen et al., 2021d).

From the perspective of engineering, visual inspection consists of human vision and machine vision.

Received 22 November 2019
Received in revised form 19 January 2022
[1] Corresponding author.
E-mail address: zhoum@tongji.edu.cn

Herein, machine vision-based inspection is designed for seeking to understand and automate tasks that the human visual system can do. The rock mass rating (RMR) is one of the most internationally recognized discrimination methods (Bieniawski, 1988), which uses the measured water inflow rate to classify the following five water inflow categories, namely completely dry, damp, wet, dripping, and flowing (listed in Table 1) (Warren et al., 2016). It is hard to distinguish the damp state and wet state by naked eyes since the rate range of damp state is less than 10 liters/min, and that of wet is 10-25 liters/min, which can only be differentiated by the flowmeter measurement. Hence, for the vision-based task, damp and wet are unified into the wet category to perform the manual image tagging. Additionally, a water gushing state is added as one of the water inflow categories because of its sudden and disastrous nature in the rock tunnelling project. Typical tunnel face images of the five water inflow categories are shown in the corresponding columns in Table 1. To provide a comprehensive assessment of water inflow status, a full surface inspection of consecutive multiple tunnel faces is essential (Cai et al., 2022; Man et al., 2022; Zarei et al., 2013). Nevertheless, the remaining challenge for the field engineers is to establish an efficient identification method of water inflow under frequently changing construction processes (Zarei et al., 2012).

Table 1. Water flow statistics and example images based on rock mass rating (RMR)

Water inflow	None	< 10 liters/min	10-25 liters/min	25-125 liters/min	>125 liters/min	Tunnel disaster
General conditions in RMR	Completely dry	Damp	Wet	Dripping	Flowing	Gushing
Classification in this study	CD	Wet		Dripping	Flowing	Gushing
Example images	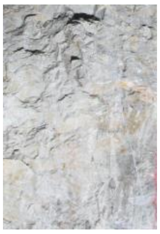				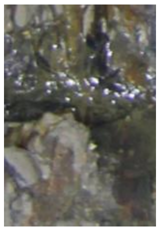	

A representative traditional visual inspection method is the geological sketch method, which is a labour-consuming task with strong subjectivity, and heavily relies on the experience and meticulousness of the inspectors (Santos et al., 2018; Sou-Sen Leu, 2011). Inspectors have to tolerate the safety risks caused by close contact with the tunnel working face to conduct the inspection and then detect potential regions of damage through stop-and-check (Cai et al., 2021). However, geological sketch methods are still widely used in many countries due to the limitations of project budgets and computational technology (Li et al., 2017; Marjoribanks, 2010).

Geological radar detection is another typical method used to identify damage by analysing medium reflection signals, which can quantify damage with a high level of automation by professional personnel, and is excellent at detecting abnormal geological environments (Annan et al., 1991; Guo et al., 2019; Koopialipoor et al., 2019b; Liu et al., 2010). However, this method urgently needs to be strengthened in terms of its sensitivity to geological hazards with little change and to simultaneously and efficiently acquire multiple comprehensive types of information, such as joints and fractures, and ground water (Chen et al., 2021a).

The latest trend is to employ computer vision methods for automated task classification (Chen et al., 2021b; Kumar et al., 2018; Nhat-Duc et al., 2018). The traditional image processing method is initially used to extract thousands of feature parameters to obtain the target characteristics with relatively backward computing equipment, to pre-design feature extractors and pre-process images before training (Chen et al., 2021a; Chen et al., 2021e). In this regard, the operational efficiency and the friendliness of the developed frameworks are undoubtedly reduced, and thus an efficient and high-precision image detection method is urgently needed.

Deep convolutional neural networks (DCNNs) have shown admirable end-to-end performance for visual detection tasks and can learn abstract features and reveal the rules of input and outputs by self-deep learning (Chen et al., 2020; Zhao et al., 2021). This method has been widely used with images for classification and detection tasks. DCNNs are made up of neurons for different functions that learn a large number of significant parameters such as weights and biases, while input data is transformed into output data (Huang et al., 2020). At present, civil engineering fields using DCNNs are primarily concentrated on the foundation pit (Fang et al., 2018), buildings (Martinez-Murcia et al., 2018; Nhat-Duc et al., 2018), shield tunnels (Huang et al., 2020; Zhou et al., 2021), and municipal utility engineering (Kumar et al., 2018), providing significant practical experience for the intellectualization and informatization of engineering construction. However, the existing research mainly focused on the operation and maintenance stages to facilitate management and repair. Few studies applied DCNNs in the under-construction site, especially for the underground excavation rock face (Lü et al., 2017).

For addressing the deficiencies as mentioned above, a digital photography method is proposed and adopted to obtain raw water inflow images (3968 × 2240 pixels) of the rock tunnel face in batches from highway tunnels under construction in Yunnan, China. Five water inflow categories (complete dry (CD), wet state (WS), dripping state (DS), flowing state (FS), and gushing state (GS)) were classified manually to establish the target image dataset. In general, the proportion of damage-free images is the largest, while the distribution of other damage images is exceptionally imbalanced, bringing the risk of over-fitting or under-fitting to the test results. Hence, a DCNN method (i.e. H-ResNet-34) employing a residual module (He et al., 2016) as the backbone framework and a hierarchical classification structure (Seo and Shin, 2019) as the multiple level classification structures is proposed to enhance the efficiency and accuracy over that of the imbalanced datasets. A resized image (229 × 229 pixels) dataset is then created, trained, validated, and tested to generate the optimal target model for water inflow classification. The water inflow classification performances of the proposed H-ResNet-34 method and the original ResNet-34 method are systematically assessed with regards to the evaluation metrics and visualization methods.

2. Water Inflow ImageNet

2.1. Image database collection

Inspired by the establishment and employment of the target ImageNet in DCNN (Deng et al., 2009), a Water Inflow ImageNet (WIIN) was built consisting of rock tunnel face images relevant to five different water inflow status: complete dry (CD), wet state (WS), dripping state (DS), flowing state (FS) and gushing state (GS). The WIIN database is used for identification and detection of water inflow problems in rock tunnel projects. To construct such a database, a digital photograph method (as shown in Fig.1, consisting of a digital camera, tapeline, tripod, light source, and measuring equipment namely laser rangefinder, thermo hygrometer, and illuminometer) is proposed for image acquisition, which can cover a variety of different rock tunnel faces. The limited lighting conditions and the cramped surrounding environment in the rock tunnel raise significant challenges for the acquisition of quality images. For improving the quality of images, two adjustable power drop LED lamps were used to increase the illumination for photographing. Additional tunnel face images were also collected from search engines like Baidu and Google to increase the image samples in the dataset, which account for approximately 20% of the total samples.

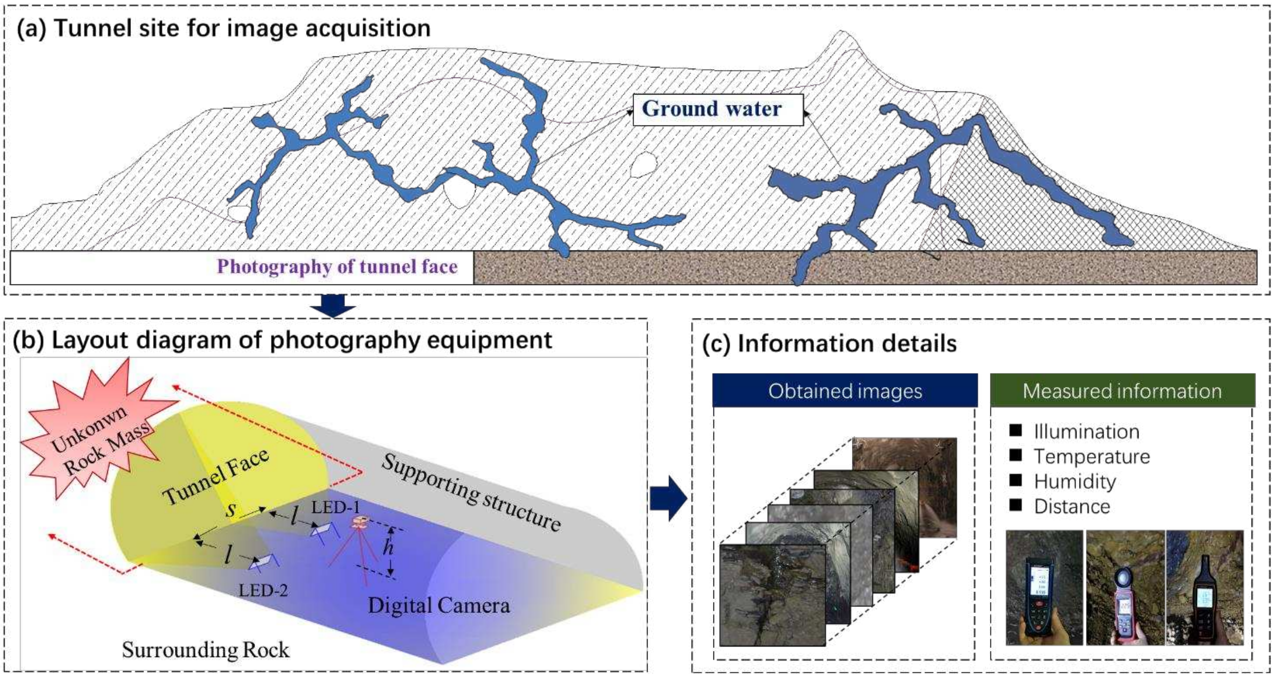

Fig. 1. Schematic diagram of the digital photograph method, including: (a) tunnel site for image acquisition, (b) layout diagram of photography equipment, and (c) information details.

2.2. Imbalanced image problem

In this study, 4012 water inflow images from various rock tunnel faces were classified manually into five categories. Sample images of the five categories of water inflow, namely CD, WS, DS, FS, and GS, are shown in Fig. 2. Because of the complex and changeable geological conditions in the highway rock tunnel, the damage texture and grey-scale distribution differences of water inflow status of various categories do not differ significantly, leading to inefficiency in the manual classification. The number of original water inflow images in each category is listed in Table 2, where the number distribution of the images is extremely imbalanced. The raw images include 2,102 non-damage (i.e. complete dry) images and 1,910 images with water inflow damage. Approximately 52% of the original images are complete dry state images without water inflow, which is three times larger than the second-largest sample size, WS, and twenty-one times larger than the smallest sample size, GS. Furthermore, the imbalance issue also exists among the images with water inflow damage. The number of WS images is seven times that of GS. Nevertheless, the issues become more challenging for multi-class classification tasks due to the existence of several minority classes. The proposed method has to balance between guaranteeing the classification rate for water inflow with typical distinctive sample scales and avoiding overfitting the minority categories. In most cases, the imbalance between different categories influences both the convergence of the training and validation processes and the generalization of the pre-trained framework on the test dataset. Hence, the imbalance problem invariably leads high classification accuracy for the majority categories, and results in low classification accuracy for the minority categories (Huang et al., 2016; Khan et al., 2017; Koopialipoor et al., 2019a; López et al., 2013).

Table 2. Water inflow categories and image dataset statistics.

Water inflow category	CD	WS	DS	FS	FS
Number of images	2,102	775	733	304	98

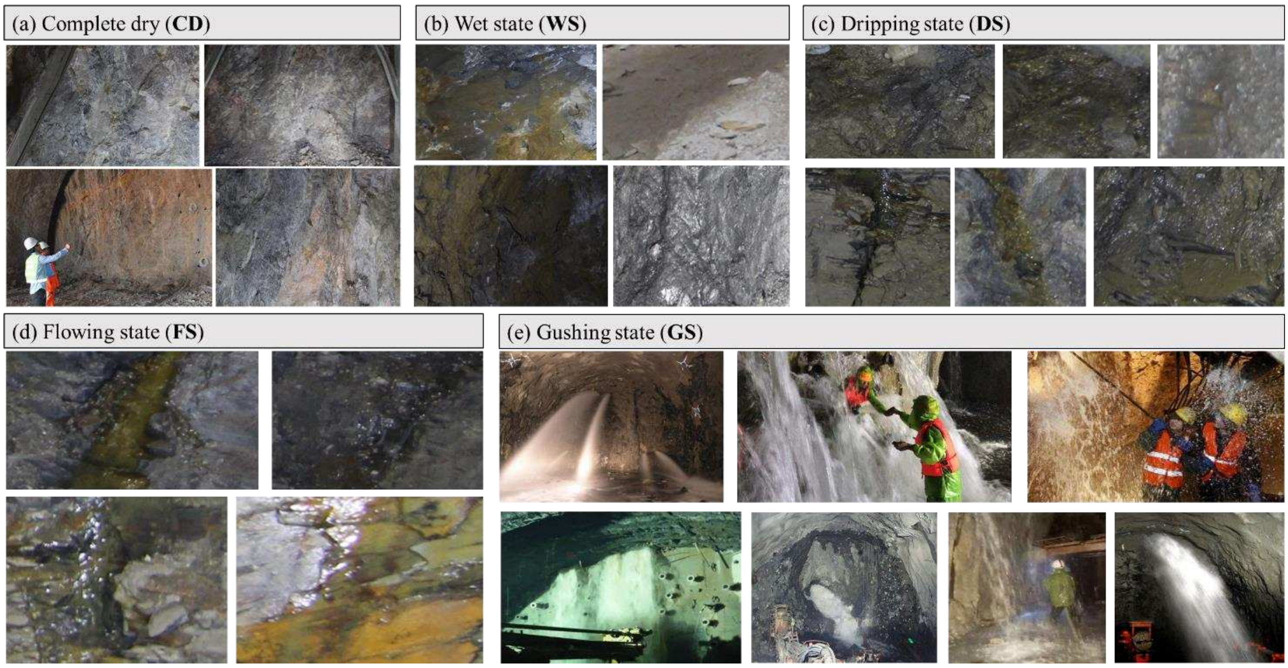

Fig. 2. Sample images for different water inflow categories: (a) complete dry (CD), (b)wet state (WS), (c) dripping state (DS), (d) flowing state (FS), and (e) gushing state (GS)

2.3. Database establishment

For relieving the imbalance issue between the images of different water inflow categories, the images with minority damage were oversampled rather than under-sampled since the over-sampling processes are proved to have better performance (López et al., 2013). In this section, some data augmentation techniques such as random blur, local amplification, random horizontal flip, Gaussian sampling, and channel scaling were selected on the raw images. Moreover, samples of minority damages were oversampled multiple times to match the balance of the proposed model. In total, 8,000 images were generated, as shown in Table 3, where the statistics of each water inflow status in the mentioned datasets are listed. To simplify analysis, the number of damaged category samples is consistent with each other, and the total number of damaged samples is equal to the non-damaged samples. Meanwhile, the proportion of training, validation, and testing dataset in each label is approximately adjusted to 60%, 25%, and 15%.

Table 3. The image numbers of training, validation, and testing datasets for different water inflow categories

Water inflow category	Training	Validation	Testing	Total number
CD	2,400	1,000	600	4,000
WS	600	250	150	1,000
DS	600	250	150	1,000
FS	600	250	150	1,000
GS	600	250	150	1,000
Total number	4,800	2,000	1,200	8,000

3 The Proposed DCNN Method

The DCNN methods have achieved excellent performance in image classification tasks, such as VGG (Chen et al., 2021c; Simonyan and Zisserman, 2014), Inception (Szegedy et al., 2015), etc. However, as the network depth increases, the performance of DCNNs gradually becomes saturated or even declines rapidly, which is known as the degradation problem of a network. To address these issues, a residual learning network (ResNet) (He et al., 2016) has shown considerably superior performance on detection rate and accuracy from the increased network depth. Meanwhile, it is much easier to optimize and modify the framework using a residual learning network instead of an unreferenced network. This study proposes a residual learning network with 34 layers (ResNet-34) as the typical backbone network to classify the water inflow images.

Furthermore, a DCNN with a hierarchical classification structure, named as H-ResNet-34, is proposed in this study to handle the afore-mentioned imbalanced water inflow image issues. Remarkably, the original ResNet-34 was modified in this study to handle hierarchical identification at both coarse-level and fine-level, that is, the H-ResNet-34 model. The coarse-level task of the framework belongs to a simple binary classification issue that classifies the damage samples from the non-damage datasets. The fine-level task then predicts the probability of each damage category by assuming at the images have damages. The hypothesises of the proposed H-ResNet-34 are that it is more efficient to classify a few categories within one category than all of the categories, and it is more efficient to train a model with balanced samples than imbalanced samples. The coarse prediction can enhance the prediction by providing the obtained fine-level features. Finally, the proposed hierarchical classifier is used to integrate the multi-level predictions to produce the final prediction results.

3.1. Base ResNet-34 model

As displayed in Fig. 3, the original ResNet-34 framework consists of five main convolution modules, which include a total of 33 convolution layers, an average pooling layer, and a fully connected (FC) layer. In order to promote the image processing efficiency, the raw images were cropped from their original sizes of 3968 × 2240 pixels into smaller resized images of 229 × 229 pixels. The first convolution module consists of a single convolution layer with 64 filters of 7×7, a stride of 2, and a padding of 3. The remaining convolution module consists of two basic residual modules.

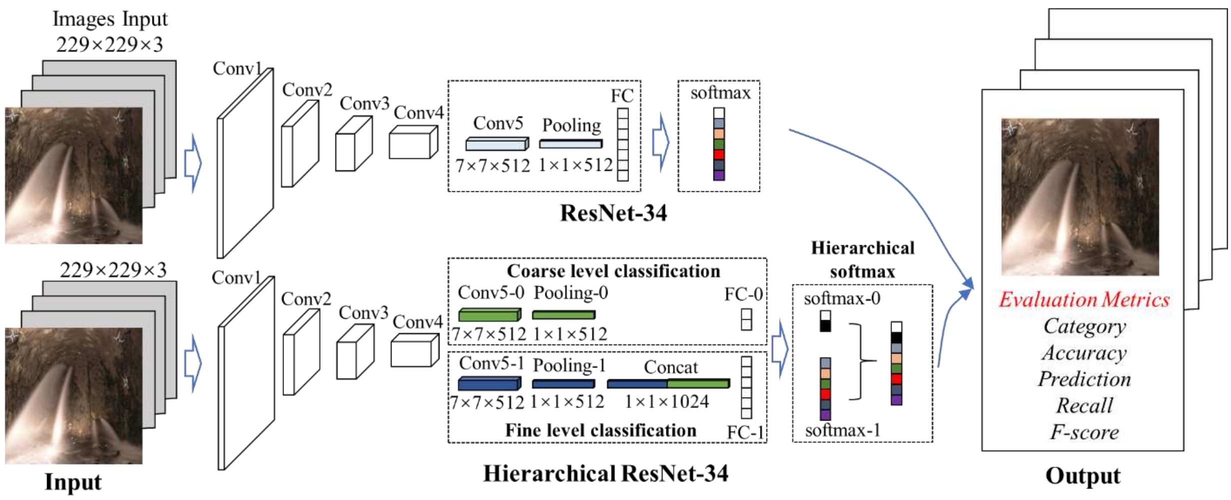

Fig. 3. The main structure of the proposed DCNN for water inflow classification, including the original ResNet-34 (on the top), and the H-ResNet-34 (at the bottom).

The residual module shown in Fig. 4 consists of two convolution layers with the same number of 3×3 filters. Each convolution module can decrease the size of the images by half and increase the feature scale in a specific range. Unlike traditional CNNs, each pair of 3×3 filters adds shortcut connection, which is applied to skip particular layers and pass raw data directly to the next layer. These new shortcut connections will not increase the parameters and the complexity of the original model, moreover the whole model can still be trained using an end-to-end approach. The configuration of each convolution module is listed in Table 4, where the final output size is 512 dimensional 1×1 filter.

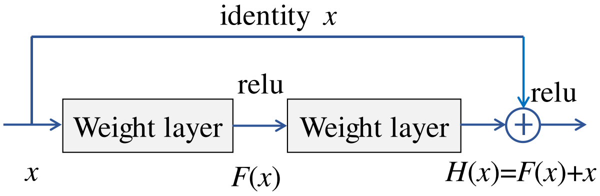

Fig. 4. Residual learning: a building module.

Table 4. H-ResNet-34 layers and configurations

Layer	Cov1	Cov2_x	Cov3_x	Cov4_x	Cov5_x	Pooling
Output size	112×112×64	56×56×56	28×28×128	14×14×256	7×7×512	1×1×512
Filters	7×7,64 stride 2	$\begin{bmatrix}3\times3,64\\3\times3,64\end{bmatrix}\times3$	$\begin{bmatrix}3\times3,128\\3\times3,128\end{bmatrix}\times4$	$\begin{bmatrix}3\times3,256\\3\times3,256\end{bmatrix}\times6$	$\begin{bmatrix}3\times3,512\\3\times3,512\end{bmatrix}\times3$	Average

Although DCNNs have achieved significant success on established benchmark datasets, they are still unable to get rid of the negative impacts caused by the imbalanced image dataset. The solution to the imbalanced issue can be divided into data-level and classifier-level methods (Buda et al., 2018; Gordan et al., 2016; Huang et al., 2016; Momeni et al., 2015). Among these, the primary process used in data-level methods is resampling, which attempts to balance the images in each category by under-sampling the main category or over-sampling the minority category. On the other hand, the classifier-level method aims to handle tasks by specific algorithms, including thresholding and ensemble learning (Buda et al., 2018; Hajihassani et al., 2015; Khan et al., 2017; Zhang et al., 2021). Therefore, a hierarchical DCNN framework, in combination with a resampling process, is adopted in this study.

Previously, several tentative hierarchical recognition algorithms (Yan et al., 2015) have shown excellent performance in visual detection on non-damage datasets. According to the hypothesis mentioned above, solving a relatively balanced binary identification issue that detects damage from a non-damage dataset is more efficient than directly detecting each individual type of damage. Undoubtedly, identifying images containing water inflow from a dataset consists of tunnel face images with water inflow damage is more efficient compared to detecting them from a dataset where both non-damage and damage images coexist. Thus, as illustrated in Fig. 3, a branch module similar to 'convolution 5' was built following 'convolution 4' to construct a hierarchical module in the original ResNet-34 framework.

The proposed identical modules in the model, named 'convolution 5-0' and 'convolution 5-1', were used for the coarse-level identification (binary classification) and the fine-level in recognition (classification of specific water inflow categories), respectively. Furthermore, the low-level features obtained by the first four convolution modules were shared and then employed as a significant basis for damage detection with the 'convolution 5' module. Thus, the features acquired from the comparatively balanced coarse-level identification were employed for the further fine-level task. Finally, the obtained coarse-level information after the average pooling layer was combined with the fine-level information to determine the final damage recognition.

3.2. Hierarchical ResNet-34 model (H-ResNet-34)

In conventional machine learning methods, predicting the probability value P_j, that one target image belongs to a specific class j, requires the calculation of the normalized value for each category. The value of P_j is computed by using a certain softmax function to obtain the unnormalized value Z_j for the corresponding category j. Then, the traditional models employ the softmax function to the last layer with T categories, as shown in Eq. (1):

$$P_c = \frac{e^{Z_c}}{\sum_{j=1}^{T} e^{Z_j}} \qquad (c \in 1, 2, \ldots., T) \tag{1}$$

In the early developments, the hierarchical structure was proposed as a natural language categorization task for the original objective to lessen the calculation cost for forecasting using large vocabularies (Morin and Bengio, 2005). It has also shown excellent performance in the classification of uncommon words. This study employed the hierarchical classification structure to solve the issue of imbalanced images. Thus, the water inflow, as shown in Fig. 5, is classified at two levels: the coarse-level and the fine-level. In the coarse level, the pre-trained images are categorized as normal images versus damage images to detect the potential damage. In the fine level, the selected images with potential damage are further classified by learning the details of different types of water inflow damage.

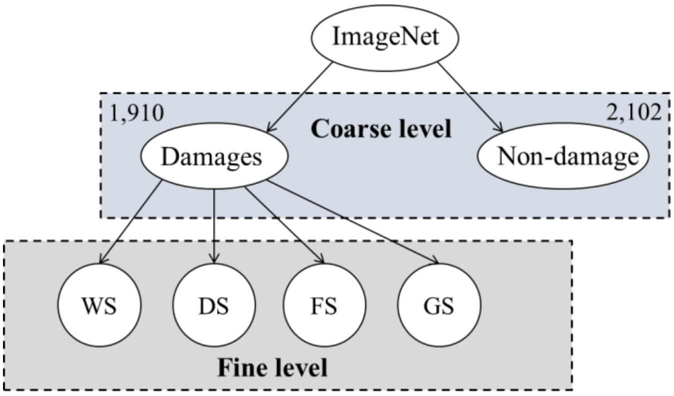

Fig. 5. Hierarchical classification of water inflow with a balanced coarse level and fine level dataset.

The probability values of each image with water inflow damage P_1 or not P_0 are obtained from the softmax-0 algorithm in the coarse-level recognition. As for the fine-level, the conditional probability $P(d_j|1)$ of individual damage d_j with softmax-1 is predicted by assuming that the images in the dataset all contain the water inflow damage. Finally, the probability values of each type of water inflow damage are computed using Eq. (2):

$$P_{d_j} = P(d_j|1) \cdot P_1 \tag{2}$$

whereas P_1 equal to 1 when it is recognized as water inflow damage in coarse recognition. By this approach, the hierarchical module can classify the water inflow category, where the final-level prediction is determined by both the coarse-level and fine-level prediction (as shown in Table 5).

Table 5. Definition of prediction probability of hierarchical structure for water inflow classification.

Prediction & Classifiers		Coarse-level	Fine-level	Final-level
		softmax-0	softmax-1	H-softmax
Categories	CD	P_0		P_0

WS	P_1	P_{WS}	P_1P_{WS}
DS		P_{DS}	P_1P_{DS}
FS		P_{FS}	P_1P_{FS}
GS		P_{GS}	P_1P_{GS}

4. Experiment and results

The proposed H-ResNet-34 framework was trained with Tensorflow (a deep learning engine specialized in CNN methods) in this study. A workstation implemented with Intel Core i7-8700 processor @3.70GHz, Nvidia GTX 1080 Ti 11GB GPU, Windows 10 operating system was employed in this research. The original ResNet-34 framework was also computed as a baseline to inspect the superiority and practicability of the proposed network. For the two DCNN methods, the epoch was terminated at 50 times, the initial learning rate was used as 0.0001, and the momentum of stochastic gradient descent (SGD) is set to 0.9.

Fig. 6 shows the main process experiment of the water inflow classification, that is, the full-cycle from data acquisition to visualization results. In the aspect of dataset preparation, it mainly contains four processes: field acquisition, image filtering and clipping, data augment, and manual classification of samples. Then the dataset goes through the training, validation, and testing processes of the two DCNN methods. Meanwhile, evaluation metrics are computed to evaluate the two DCNN methods. Finally, the two methods are visualized through feature maps, random selected image classification, and confusion matrix to demonstrate the corresponding performances.

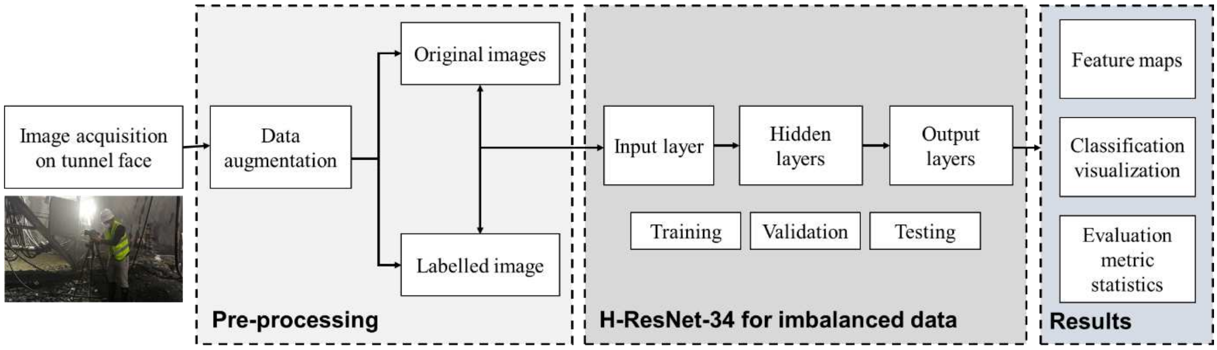

Fig. 6. The main process experiment of the water inflow classification

4.1 Evaluation metrics of experiment

The evaluation metrics, namely total loss, accuracy, precision, recall, and F-score are frequently applied in the training, validation, and testing processes to evaluate the performance of the proposed classification methods. The correlation between the evaluation metrics and the essential metrics (i.e., true positive (TP), true negative (TN), false positive (FP), and false negative (FN)) are presented in Eqs. (3-6).

The accuracy metric is the proportion of accurately classified samples in all tasks, which can be computed as follows:

$$Accuracy = \frac{TP + TN}{TP + TN + FP + FN} \tag{3}$$

The precision metric is the proportion of true positives in all the samples marked as positive. It is calculated as follows:

$$Precision = \frac{TP}{TP + FP} \tag{4}$$

The recall metric presents the proportion of true positive in all positive samples, that is, the reflection of samples correctly labelled as positive in the target:

$$Recall = \frac{TP}{TP + FN} \tag{5}$$

The F-score metric is a comprehensive indicator calculated by a specific way between recall and precision:

$$F_{\alpha} = \frac{(\alpha^2 + 1) Precision \times Recall}{\alpha^2 (Precision \times Recall)} \tag{6}$$

where α value is set as 1 in this study, which reflects the significance of recall and precision is the same.

4.2. Training and validation results

In both DCNN methods, 4,800 and 2,000 water inflow images are selected for the processes of training and validation, respectively. To further reveal the feature extraction process during the training process, the feature maps of water inflow images are shown in Fig. 7. Among them, basic features, such as corner, texture, and edge, are extracted through the low-level features. The middle-layer then checks the motifs by observing the arrangements of the low-level image features. As a result, more feature combinations can be assembled from the motifs by the high-level layer, and the water inflow categories can then be classified.

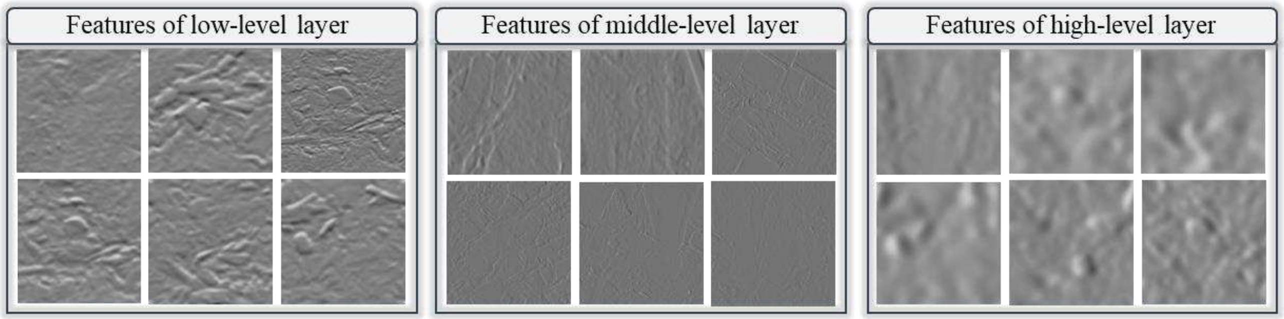

Fig. 7. Feature maps of water inflow images during the training process generated by the DCNNs.

The total loss curves are plotted in Fig. 8 to quantitatively measure the fitting degree and convergence of the target DCNNs (ResNet-34 and H-ResNet-34). It is reported in Fig. 8 that both DCNN methods converge in the training and validation processes, and the total loss curve of H-ResNet-34 converges faster than ResNet-34 in both the training and validation processes.

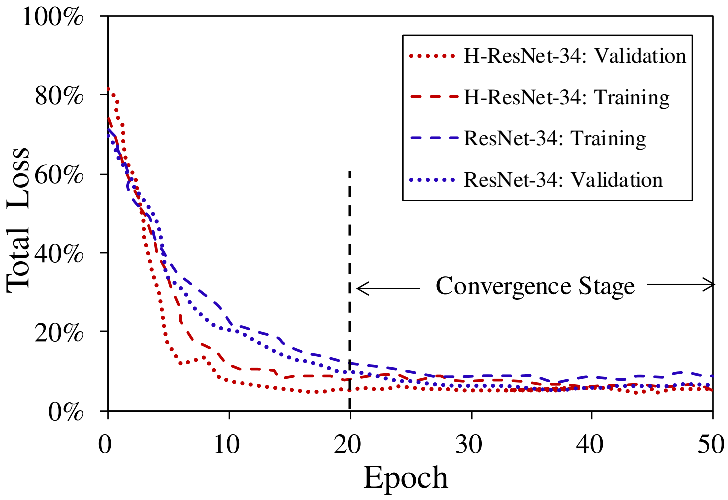

Fig. 8. Performance of both DCNN methods for total loss in training and validation processes.

4.3 Testing results

By the allocated dataset distribution, the testing dataset consists of 1,200 randomly selected images. The testing images are classified through the trained and validated DCNN methods (ResNet-34 and H-ResNet-34). Six images out of the 1,200 testing images for each DCNN method are chosen, and the corresponding classification confidences are presented in Fig. 9. Overall, H-ResNet-34 presents a better performance than ResNet-34. The classification confidence of both DCNN methods for the five water inflow categories is highest for the GS category and followed by the CD category.

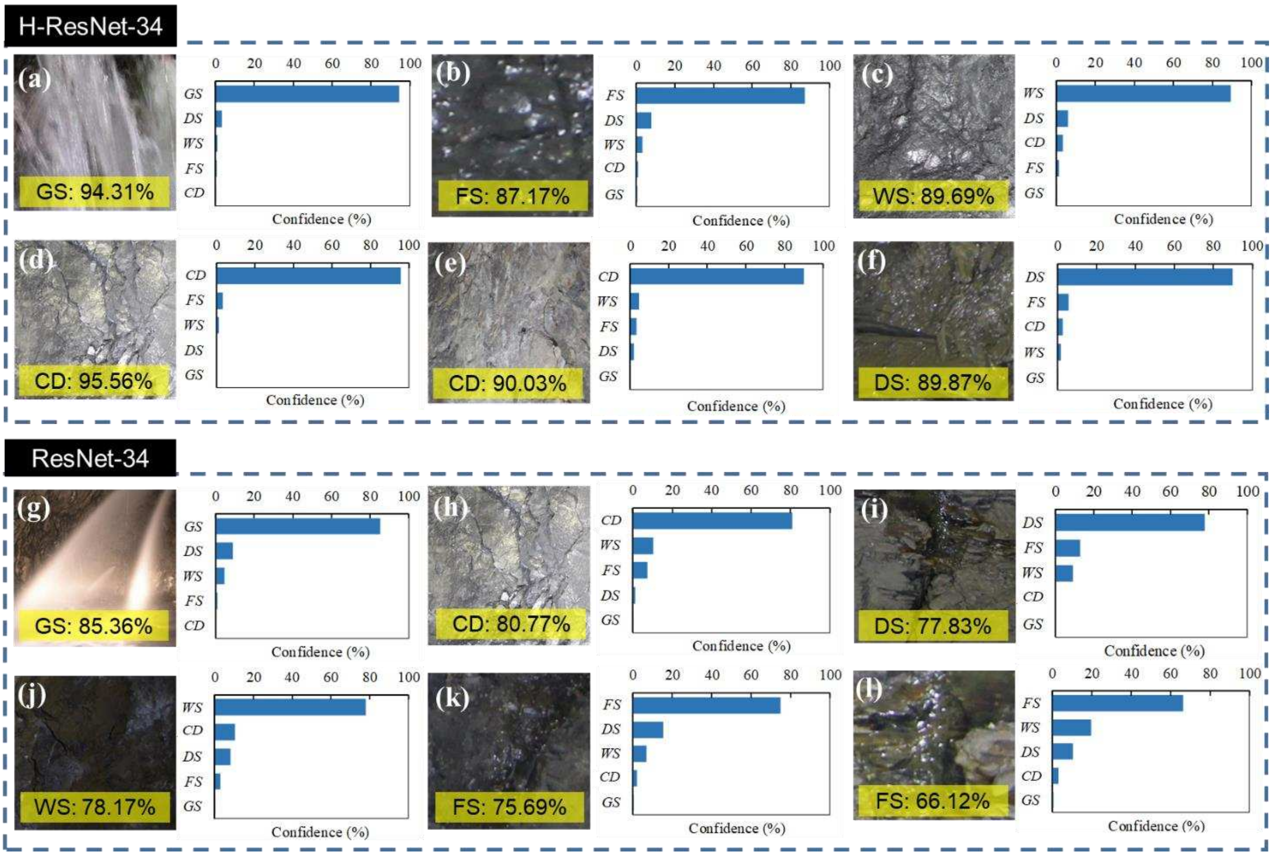

Fig. 9. Classification results of randomly selected water inflow images: (a) to (f) with H-ResNet-34, (g) to (l) with ResNet-34.

To present an informative comparison, a confusion matrix is computed in this study (shown in Fig. 10). A confusion matrix is a standard form of matrix form with n rows and n columns to express classification performance, where the n is assumed as the total number of categories. By quantitatively comparing the confusion matrixes between two DCNN methods, the proposed H-Resnet-34 shows excellent improvement in the classification of the water inflow categories. The GS category has the highest true positive probability of 95.33%, followed by CD, WS, DS, and FS categories with probabilities of 94.17%, 91.33%, 90.00%, and 88.00%, respectively. By investigating the misclassification between different water inflow categories, DS has a 9.34% probability of being misclassified as FS, 0and FS has a 7.33% probability of being misjudged as DS. The relatively high misjudgment probabilities between DS and FS are due to similar subtle textures and grey values in the sample images of the DS and FS categories. Thus, it is urgent to increase the DS and FS image dataset and enhance the texture morphology identification in the training process.

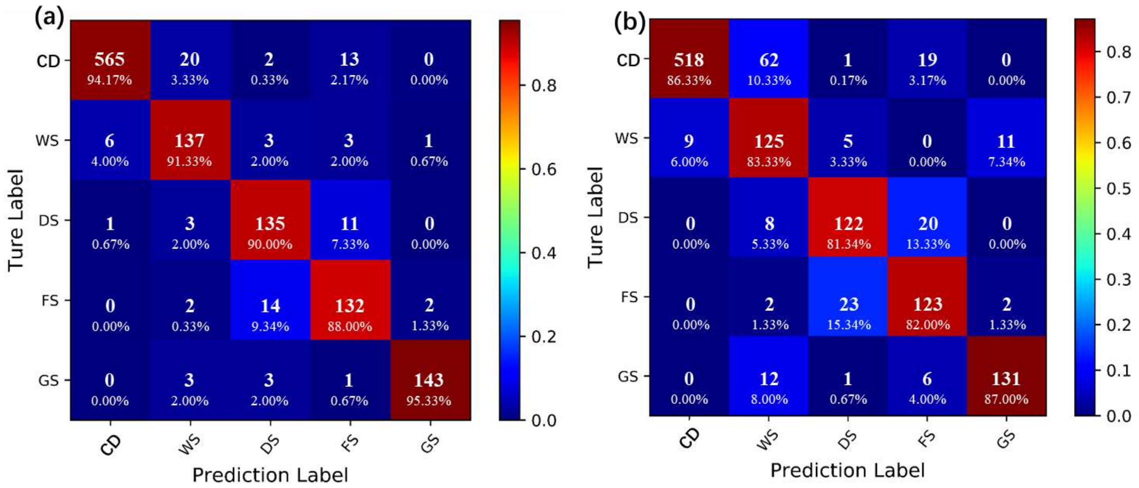

Fig. 10. Confusion matrixes of the testing dataset classification results: (a) with H-ResNet-34, (b) with ResNet-34.

For further quantitative analysis, Fig 11 plots the comparison between the original ResNet-34 and the H-Resnet-34 in terms of accuracy, precision, recall value, and F-score for both validation and testing dataset. All the evaluation metrics of both DCNN methods present a similar trend. The values of the metrics from the highest to the lowest always follow the same order: GS, CD, WS, DS, and FS. Since the texture features and distinct appearance of the GS images, it makes the DCNN methods corresponding more prominent in GS identification. The classification of DS and FS images suggest relatively poor performance, as the evaluation metrics of these two categories present rather low values. The potential reason is that the DS and FS images in the dataset do not have distinct features compared with the other three water in flow categories. By computing the mean values of precision, recall, and F-score, the corresponding values of H-Resnet-34 suggest 7.5%, 4.6%, and 6.7% higher than those of the original ResNet-34 method, respectively. Overall, adding a hierarchical structure to the original ResNet-34 can improve the classification accuracy on an imbalanced image dataset. Moreover, in the deep learning classification process, relatively low accuracy occurs in two categories with similar textures (e.g., DS and FS).

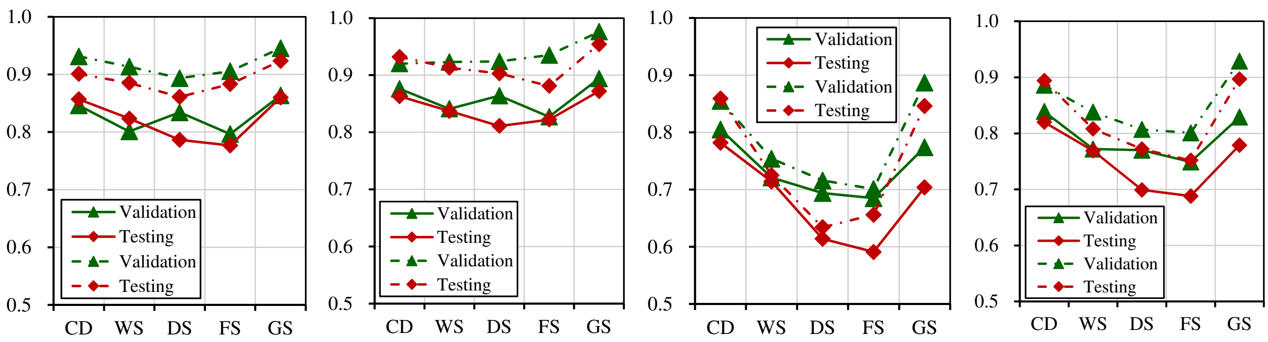

(a) Accuracy (b) Precision (c) Recall (d) F-score

Fig. 10. Performance of both DCNN methods in validation and testing processes (solid line for ResNet-34, dotted line for H-ResNet-34): (a) accuracy, (b) precision, (c) recall, and (d) F-score.

5. Conclusion

A vision-based automated method for classification of water inflow damage from imbalanced images of under-construction tunnel faces was proposed, employing a deep convolutional neural network. For solving the issue of extremely imbalanced image datasets, the ResNet-34 framework was employed as the backbone network and was then modified with a hierarchical classification structure to classify damage at two different levels: coarse-level and fine-level. The coarse-level identification, which could be simplified to a binary problem, was used to distinguish the dataset of images with water inflow damage from non-damage images. Then the fine-level identification was applied to compute the occurrence probability of each type of damage. The two branches were finally gathered to acquire the ultimate results of each type of damage based on the defined conditional probability.

The proposed H-ResNet-34 model consists of five convolution modules, an average pooling layer, and two hierarchical classification modules. It was trained, validated, and tested on the resized images captured by a digital photography method in highway tunnels under construction in Yunnan, China. The images within minority categories were first oversampled, and then the dataset was increased using augmentation techniques. The experimental results revealed that the proposed classifier could significantly improve the final accuracy of water inflow classification.

The misjudgment rate between DS and FS is relatively high due to similar subtle textures and grey values in the sample images of these two categories. Thus, it is urgent to strengthen the robustness of the imbalanced dataset to handle the typical error identification that mainly occurs in two categories with similar textures. In order to achieve higher accuracy and efficiency in the minority categories, increasing the number of samples within each category and identifying more texture morphology are both required for future research

Acknowledgments

The research presented in this paper is supported by Key innovation team program of innovation talents promotion plan by MOST of China (No. 2016RA4059), Natural Science Foundation Committee Program of China (Grant No. 1538009, Grant No. 51778474), Science and Technology Project of Yunnan Provincial Transportation Department (No. 25 of 2018), and the Fundamental Research Funds for the Central Universities of China (Grant No. 0200219129).

References

Annan, A., Cosway, S., Redman, J., 1991. Water table detection with ground-penetrating radar, SEG Technical Program Expanded Abstracts 1991. Society of Exploration Geophysicists, pp. 494-496.

Bieniawski, Z., 1988. The rock mass rating (RMR) system (geomechanics classification) in engineering practice, Rock Classification Systems for Engineering Purposes. ASTM International.

Buda, M., Maki, A., Mazurowski, M.A., 2018. A systematic study of the class imbalance problem in convolutional neural networks. Neural Networks. 106, 249-259.

Cai, W., Zhu, H., Liang, W., 2022. Three-dimensional tunnel face extrusion and reinforcement effects of underground excavations in deep rock masses. International Journal of Rock Mechanics and Mining Sciences. 150, 104999.

Cai, W., Zhu, H., Liang, W., Zhang, L., Wu, W., 2021. A New Version of the Generalized Zhang–Zhu Strength Criterion and a Discussion on Its Smoothness and Convexity. Rock Mechanics and Rock Engineering. 1-17.

Chen, J., Huang, H., Cohn, A.G., Zhang, D., Zhou, M., 2021a. Machine learning-based classification of rock discontinuity trace: SMOTE oversampling integrated with GBT ensemble learning. International Journal of Mining Science and Technology.

Chen, J., Yang, T., Zhang, D., Huang, H., Tian, Y., 2021b. Deep learning based classification of rock structure of tunnel face. Geoscience Frontiers. 12(1), 395-404.

Chen, J., Zhang, D., Huang, H., Shadabfar, M., Zhou, M., Yang, T., 2020. Image-based segmentation and quantification of weak interlayers in rock tunnel face via deep learning. Automation in Construction. 120, 103371.

Chen, J., Zhou, M., Huang, H., Zhang, D., Peng, Z., 2021c. Automated extraction and evaluation of fracture trace maps from rock tunnel face images via deep learning. International Journal of Rock Mechanics and Mining Sciences. 142, 104745.

Chen, J., Zhou, M., Zhang, D., Huang, H., Zhang, F., 2021d. Quantification of water inflow in rock tunnel faces via convolutional neural network approach. Automation in Construction. 123, 103526.

Chen, J., Zhou, M., Zhang, D., Huang, H., Zhang, F., 2021e. Towards automatic quantification of water inflow in rock tunnel faces via a novel CNN approach. Automation in Construction.

Deng, J., Dong, W., Socher, R., Li, L.-J., Li, K., Fei-Fei, L., 2009. Imagenet: A large-scale hierarchical image database, 2009 IEEE conference on computer vision and pattern recognition. Ieee, pp. 248-255.

Fang, W., Ding, L., Zhong, B., Love, P.E.D., Luo, H., 2018. Automated detection of workers and heavy equipment on construction sites: A convolutional neural network approach. Advanced Engineering Informatics. 37, 139-149.

Fernandez, G., Moon, J., 2010. Excavation-induced hydraulic conductivity reduction around a tunnel–Part 1: Guideline for estimate of ground water inflow rate. Tunnelling and Underground Space Technology. 25(5), 560-566.

Gordan, B., Armaghani, D.J., Hajihassani, M., Monjezi, M., 2016. Prediction of seismic slope stability through combination of particle swarm optimization and neural network. Engineering with Computers. 32(1), 85-97.

Guo, H., Zhou, J., Koopialipoor, M., Armaghani, D.J., Tahir, M., 2019. Deep neural network and whale optimization algorithm to assess flyrock induced by blasting. Engineering with Computers. 1-14.

Hajihassani, M., Armaghani, D.J., Marto, A., Mohamad, E.T., 2015. Ground vibration prediction in quarry blasting through an artificial neural network optimized by imperialist competitive algorithm. Bulletin of Engineering Geology and the Environment. 74(3), 873-886.

He, K., Zhang, X., Ren, S., Sun, J., 2016. Deep residual learning for image recognition, Proceedings of the IEEE conference on computer vision and pattern recognition, pp. 770-778.

Huang, C., Li, Y., Change Loy, C., Tang, X., 2016. Learning deep representation for imbalanced classification, Proceedings of the IEEE conference on computer vision and pattern recognition, pp. 5375-5384.

Huang, H., Cheng, W., Zhou, M., Chen, J., Zhao, S., 2020. Towards Automated 3D Inspection of Water Leakages in Shield Tunnel Linings Using Mobile Laser Scanning Data. Sensors. 20(22), 6669.

Hwang, J.-H., Lu, C.-C., 2007. A semi-analytical method for analyzing the tunnel water inflow. Tunnelling and Underground Space Technology. 22(1), 39-46.

Khan, S.H., Hayat, M., Bennamoun, M., Sohel, F.A., Togneri, R., 2017. Cost-sensitive learning of deep feature representations from imbalanced data. IEEE transactions on neural networks and learning systems. 29(8), 3573-3587.

Koopialipoor, M., Fahimifar, A., Ghaleini, E.N., Momenzadeh, M., Armaghani, D.J., 2019a. Development of a new hybrid ANN for solving a geotechnical problem related to tunnel boring machine performance. Engineering with Computers. 1-13.

Koopialipoor, M., Ghaleini, E.N., Haghighi, M., Kanagarajan, S., Maarefvand, P., Mohamad, E.T., 2019b. Overbreak prediction and optimization in tunnel using neural network and bee colony techniques. Engineering with Computers. 35(4), 1191-1202.

Kumar, S.S., Abraham, D.M., Jahanshahi, M.R., Iseley, T., Starr, J., 2018. Automated defect classification in sewer closed circuit television inspections using deep convolutional neural networks. Automation in Construction. 91, 273-283.

Li, S., Liu, B., Xu, X., Nie, L., Liu, Z., Song, J., Sun, H., Chen, L., Fan, K., 2017. An overview of ahead geological prospecting in tunneling. Tunnelling and Underground Space Technology. 63, 69-94.

Liu, S., Wu, J., Zhou, J., Zeng, Z., 2010. Numerical simulations of borehole radar detection for metal ore. IEEE Geoscience and Remote Sensing Letters. 8(2), 308-312.

López, V., Fernández, A., García, S., Palade, V., Herrera, F., 2013. An insight into classification with imbalanced data: Empirical results and current trends on using data intrinsic characteristics. Information sciences. 250, 113-141.

Lü, Q., Xiao, Z.-P., Ji, J., Zheng, J., Shang, Y.-Q., 2017. Moving least squares method for reliability assessment of rock tunnel excavation considering ground-support interaction. Computers and Geotechnics. 84, 88-100.

Man, J., Huang, H., Ai, Z., Chen, J., 2022. Analytical model for tunnel face stability in longitudinally inclined layered rock masses with weak interlayer. Computers and Geotechnics. 143, 104608.

Marjoribanks, R., 2010. Geological methods in mineral exploration and mining. Springer Science & Business Media.

Martinez-Murcia, F.J., Gorriz, J.M., Ramirez, J., Ortiz, A., 2018. Convolutional Neural Networks for Neuroimaging in Parkinson's Disease: Is Preprocessing Needed? Int J Neural Syst. 28(10), 1850035.

Momeni, E., Armaghani, D.J., Hajihassani, M., Amin, M.F.M., 2015. Prediction of uniaxial compressive strength of rock samples using hybrid particle swarm optimization-based artificial neural networks. Measurement. 60, 50-63.

Morin, F., Bengio, Y., 2005. Hierarchical probabilistic neural network language model, Aistats. Citeseer, pp. 246-252.

Nhat-Duc, H., Nguyen, Q.-L., Tran, V.-D., 2018. Automatic recognition of asphalt pavement cracks using metaheuristic optimized edge detection algorithms and convolution neural network. Automation in Construction. 94, 203-213.

Rálek, P., Hokr, M., 2013. Methods of Water Inflow Measurement in the Bedřichov Tunnel. EGRSE. Explor. Geophys., Remote Sens. Environment. 2, 30-39.

Santos, V., da Silva, P., Brito, M., 2018. Estimating RMR Values for Underground Excavations in a Rock Mass. Minerals. 8(3), 78.

Seo, Y., Shin, K.-s., 2019. Hierarchical convolutional neural networks for fashion image classification. Expert Systems with Applications. 116, 328-339.

Simonyan, K., Zisserman, A., 2014. Very deep convolutional networks for large-scale image recognition. arXiv preprint arXiv:1409.1556.

Sou-Sen Leu, A.T.J.W., 2011. Probabilistic prediction of tunnel geology using a Hybrid Neural-HMM. Engineering Applications of Artificial Intelligence. 24(4), 658-665.

Szegedy, C., Liu, W., Jia, Y., Sermanet, P., Reed, S., Anguelov, D., Erhan, D., Vanhoucke, V., Rabinovich, A., 2015. Going deeper with convolutions, Proceedings of the IEEE conference on computer vision and pattern recognition, pp. 1-9.

Warren, S.N., Kallu, R.R., Barnard, C.K., 2016. Correlation of the Rock Mass Rating (RMR) System with the Unified Soil Classification System (USCS): Introduction of the Weak Rock Mass Rating System (W-RMR). Rock Mechanics and Rock Engineering. 49(11), 4507-4518.

Yan, Z., Zhang, H., Piramuthu, R., Jagadeesh, V., DeCoste, D., Di, W., Yu, Y., 2015. HD-CNN: hierarchical deep convolutional neural networks for large scale visual recognition, Proceedings of the IEEE international conference on computer vision, pp. 2740-2748.

Zarei, H., Uromeihy, A., Sharifzadeh, M., 2013. A new tunnel inflow classification (TIC) system through sedimentary rock masses. Tunnelling and underground space technology. 34, 1-12.

Zarei, H.R., Uromeihy, A., Sharifzadeh, M., 2012. Identifying geological hazards related to tunneling in carbonate karstic rocks-Zagros, Iran. Arabian Journal of Geosciences. 5(3), 457-464.

Zhang, J.-Z., Phoon, K.K., Zhang, D.-M., Huang, H.-W., Tang, C., 2021. Novel approach to estimate vertical scale of fluctuation based on CPT data using convolutional neural networks. Engineering Geology. 294, 106342.

Zhao, S., Zhang, D., Xue, Y., Zhou, M., Huang, H., 2021. A deep learning-based approach for refined crack evaluation from shield tunnel lining images. Automation in Construction. 132, 103934.

Zhou, M., Cheng, W., Huang, H., Chen, J., 2021. A novel approach to automated 3d spalling defects inspection in railway tunnel linings using laser intensity and depth information. Sensors. 21(17), 5725.